# Fast Computation, Rotation, and Comparison of Low Resolution Spherical Harmonic Molecular Surfaces

**DAVID W. RITCHIE,[1,2] GRAHAM J. L. KEMP[1]**

[1]*Department of Computing Science, King's College, University of Aberdeen, Aberdeen AB24 3UE, United Kingdom*

[2]*Department of Molecular and Cell Biology, Polwarth Building, University of Aberdeen, Aberdeen AB25 2ZD, United Kingdom*

*Received 30 June 1997; revised 3 July 1998; accepted 8 July 1998*

**ABSTRACT:** A procedure that rapidly generates an approximate parametric representation of macromolecular surface shapes is described. The parametrization is expressed as an expansion of real spherical harmonic basis functions. The advantage of using a parametric representation is that a pair of surfaces can be matched by using a quasi-Newton algorithm to minimize a suitably chosen objective function. Spherical harmonics are a natural and convenient choice of basis function when the task is one of search in a rotational search space. In particular, rotations of a molecular surface can be simulated by rotating only the harmonic expansion coefficients. This rotational property is applied for the first time to the 3-dimensional molecular similarity problem in which a pair of similar macromolecular surfaces are to be maximally superposed. The method is demonstrated with the superposition of antibody heavy chain variable domains. Special attention is given to computational efficiency. The spherical harmonic expansion coefficients are determined using fast surface sampling and integration schemes based on the tessellation of a regular icosahedron. Low resolution surfaces can be generated and displayed in under 10 s and a pair of surfaces can be maximally superposed in under 3 s on a contemporary workstation.  J Comput Chem 20: 383–395, 1999

**Keywords:** molecular similarity; surface shape; spherical harmonics; real rotation matrices; icosahedral sampling; icosahedral integration; function minimization

*Correspondence to:* Dr. D. W. Ritchie; e-mail: dritchie@csd.abdn.ac.uk



CCC 0192-8651 / 99 / 040383-13

## Introduction

Molecular surface shape plays a significant role in protein–protein and protein–ligand interactions. For example, surface shape complementarity is usually a necessary condition for protein–ligand binding and is often the main discriminant in rigid body docking simulations. Finding the best superposition of ligand shapes is normally the first step in the quantitative structure–activity relationship method of *de novo* drug design.

There are many techniques for modeling molecular surface shape. These often begin with a strictly geometric interpretation of the surface atoms in a hard sphere model of the molecule to give the familiar solvent-accessible[1] and molecular surfaces.[2] Representing these surfaces as dots, triangles, or analytical surface segments[3–5] can be an effective way to visualize the surface shape. However, such representations contain much high resolution detail and so are not particularly convenient computational forms when the task is to search for regions of similarity or complementarity between a pair of molecules. The molecular surfaces may be contoured or sliced to find local maxima and minima,[6] surface normals or solid angles can be calculated,[4,7] and the search for complementary shapes can then be expressed in terms of matching ''knobs to holes''[6,8] or matching opposing surface normals.[9,10] However, assuming rigid bodies, there are 6 degrees of freedom in the docking problem and often the entire geometric representation must be rotated and translated for each trial orientation. Clever indexing schemes can be used to reduce the amount of computation[9,11] as can an intelligent choice of surface normals,[12,13] but nonetheless most surface matching procedures still need to generate and test many thousands of possible orientations. Even in the much simpler case of the molecular similarity problem, which we focus on here, the 3 rotational degrees of freedom make the search space nontrivial.

An alternative to the ''generate and test'' approach is to direct the course of the search using function minimization. An objective function is chosen to represent the state of the system, and this is minimized to find the most favorable orientation. This approach can be made tractable with a suitably approximate parametric representation of the surface from which surface quantities can be derived as needed. Because the general docking problem can be expressed in terms of a translation and 5 rotational degrees of freedom,[14] the similarity and the docking problems can both be considered in terms of search in a ''rotational search space.'' Thus, it is natural to seek a parametric representation that is robust under rotation; it is for this reason that we chose to represent a molecular surface as an expansion of spherical harmonic functions. This idea is not new: Max and Getzoff[15] showed that low order harmonic functions can capture the gross features of a molecular surface. Duncan and Olson[16] and Leicester et al.[17] generated high resolution surface expansions that begin to reproduce the exact atomic detail of the surface. Although many useful surface properties can be derived from a spherical harmonic representation[16] and the rotation of surface expansion coefficients has been considered,[17] it appears that further investigation of spherical harmonic molecular surfaces may have been deterred by the computational cost reported in these earlier studies.

Here the rotational properties of spherical harmonics are used for the first time to match similar molecular surface shapes. We address the problem of computational efficiency by reviewing and reformulating some of the expressions used in the literature and by using a cache of intermediate values. We also introduce a simple but novel integration scheme, which is based on an icosahedral tessellation of the sphere, that rapidly calculates the initial surface expansion coefficients. The symmetry of the icosahedron was exploited before in relation to surface sampling[18,19] and comparison,[18] rotational search,[20] and as a visualization tool.[21,22] Our sampling and integration algorithms were largely inspired by these articles.

Because many protein domains are essentially globular in shape and most of the shape information can be encoded in the first few harmonic coefficients,[23] we chose to use relatively low order surface expansions and to assume a single-valued surface (i.e., we do not attempt to model reentrant surfaces correctly). When a single-valued surface is assumed, we can use a fast surface sampling scheme, again based on the icosahedron, to give very good estimates of the solvent-accessible and molecular surfaces directly from the 3-dimensional structure. We then exploit the rotational properties of spherical harmonics to systematically rotate the surface coefficients, allowing a rapid search for the global minimum of a shape similarity function.

The method is demonstrated using antibody heavy chain variable (VH) domains. Antibody domains have highly conserved $\beta$-sheet framework regions, although the variable domains of Fv frag-

ments present a variety of surface shapes due to differences in the hypervariable loop regions of their complementarity determining regions (CDRs). Hence, the shapes of these domains have sufficient differences to provide a good test of our surface shape matching algorithm, yet are sufficiently similar that the quality of a surface shape superposition is easily recognized by observing the relative positions of the corresponding backbone traces. We show that it is possible to generate spherical harmonic surfaces of two randomly oriented antibody domains and to find the best superposition of these surfaces in a matter of seconds on a modern workstation. Our results indicate that low resolution spherical harmonic molecular surfaces can be calculated remarkably quickly, and we suggest that the resulting parametrization may be a useful computational tool in many aspects of protein surface shape analysis.

## Methods

A single-valued surface in 3-dimensional (3-D) space can be parametrized by the spherical coordinates, $(\theta, \phi)$, such that all points, $\underline{\mathbf{x}}$, on the surface are given by

$$\underline{\mathbf{x}}(\theta, \phi) = r(\theta, \phi)\left[\sin\theta\cos\phi\,\underline{\mathbf{i}} + \sin\theta\sin\phi\,\underline{\mathbf{j}} + \cos\theta\,\underline{\mathbf{k}}\right], \quad (1)$$

where the radial function, $r(\theta, \phi)$, encodes the distance of surface points from a chosen origin. The classical way to determine such a function is to write it as an expansion of spherical harmonic basis functions,[24]

$$r(\theta, \phi) = \sum_{l=0}^{L} \sum_{m=-l}^{l} a_{lm} Y_{lm}(\theta, \phi) \quad (2)$$

and to solve for the expansion coefficients, $a_{lm}$ (discussed below). The upper limit, $L$, is chosen to give the desired level of resolution; a value of $L = 30$ can resolve surface detail to around 1Å on the surface of a typical protein domain.[16]

### COMPLEX SPHERICAL HARMONICS

The mathematics of spherical harmonics are well known (see, e.g., Biedenharn and Louck[25] for a detailed and authoritative account), so here we merely summarize some of the properties that are relevant to the description of molecular surfaces, particularly with respect to rotation. In their general form, spherical harmonics are complex orthonormal functions that are often written in terms of the spherical coordinates $(\theta, \phi)$, because these variables can be separated to give a product of functions

$$Y_{lm}(\theta, \phi) = \vartheta_{lm}(\theta)\varphi_m(\phi) \quad -l \le m \le +l \quad (3)$$

where

$$\vartheta_{lm}(\theta) = \left[\frac{(2l+1)}{2}\frac{(l-m)!}{(l+m)!}\right]^{1/2} P_l^m(\theta), \quad (4)$$

$$\varphi_m(\phi) = [2\pi]^{-1/2} e^{im\phi}. \quad (5)$$

The functions $P_l^m(\theta)$ are the associated Legendre polynomials. The square root terms are normalization factors such that the orthonormality property can be expressed as

$$\int_0^{2\pi}\int_0^{\pi} Y_{lm}(\theta, \phi) Y_{kj}(\theta, \phi)^* \sin\theta\, d\theta\, d\phi = \delta_{lk}\delta_{mj} \quad (6)$$

where the asterisk denotes complex conjugation. As indicated above, one of the many applications of spherical harmonics is to use them as a basis set in which functions of $(\theta, \phi)$ can be expanded. Here we have a radial distance function, $r(\theta, \phi)$, although any other surface property could be represented in the same way. The coefficients of the harmonic expansion are found using the orthonormality property; multiplying each side of eq. (2) by the complex conjugate, $Y_{lm}(\theta, \phi)^*$, and integrating over the sphere gives an integral for each coefficient:

$$a_{lm} = \int_0^{2\pi}\int_0^{\pi} r(\theta, \phi) Y_{lm}(\theta, \phi)^* \sin\theta\, d\theta\, d\phi. \quad (7)$$

There are $(L+1)^2$ such integrals for an expansion to order $L$ and generally each integral must be evaluated numerically. This is often a costly operation,[26] although not especially so with our algorithm. In any case, the integrals need only be evaluated once; the operation of a rotation on the molecule (or conversely, a rotation of the coordinate system) can be simulated by transforming only the expansion coefficients.

The spherical harmonic basis functions of each order, $(l)$, transform among themselves under rotation according to[25]

$$\hat{R}(\alpha\beta\gamma)Y_{lm}(\theta,\phi) = \sum_{m'} Y_{lm'}(\theta,\phi)D^{(1)}_{m'm}(\alpha\beta\gamma), \tag{8}$$

where $\hat{R}(\alpha\beta\gamma)$ represents a rotation operator expressed in terms of the Euler angle parametrization $(\alpha\beta\gamma)$. The unitary rotation matrices $D^{(l)}(\alpha\beta\gamma)$ are due to Wigner and the matrix elements are given by

$$D^{(l)}_{m'm}(\alpha\beta\gamma) = e^{-im'\alpha}d^{(l)}_{m'm}(\beta)e^{-im\gamma}, \tag{9}$$

where

$$\begin{aligned} d^{(l)}_{m'm}(\beta) &= \left[\frac{(1+m')!}{(l+m)!}\frac{(l-m')!}{(l-m)!}\right]^{1/2} \\ &\times \sum_{k=\max(0,\,m-m')}^{\min(l-m',\,l+m)} \left[(-1)^{k+m'-m}\binom{l+m}{k}\right. \\ &\times \binom{l-m}{l-m'-k} \\ &\left.\times(\cos\beta/2)^{2l+m-m'-2k}(\sin\beta/2)^{2k+m'-m}\right]. \end{aligned} \tag{10}$$

Because the harmonic basis functions transform among themselves, it follows that the coefficients of a surface expansion must also. Rotating $r(\theta,\phi)$ gives some new function, $r'(\theta,\phi)$, that represents the same surface but in a different orientation:

$$r'(\theta,\phi) = \hat{R}(\alpha\beta\gamma)r(\theta,\phi). \tag{11}$$

Substituting the appropriate harmonic expansion for each side gives

$$\sum_{lm} a'_{lm}Y_{lm}(\theta,\phi) = \sum_{l'm'} a_{l'm'}\sum_{q} Y_{l'q}(\theta,\phi)D^{(l)}_{qm'}(\alpha\beta\gamma), \tag{12}$$

and on multiplying both sides by $Y_{kj}(\theta,\phi)^*$ and integrating over the sphere, all terms vanish except $k = l = l'$ and $j = m = q$ to give

$$a'_{lm} = \sum_{m'} a_{lm'}D^{(l)}_{mm'}(\alpha\beta\gamma). \tag{13}$$

That is, the harmonic expansion coefficients transform among themselves under rotation in a similar way in which rotations transform the $(x, y, z)$ coordinates in the Cartesian frame. Clearly, this holds for the coefficients of any spherical harmonic parametrization, not just of $r(\theta,\phi)$. This fundamental property was recognized by Leicester et al.,[17] although they were unsuccessful in implementing a surface matching scheme that could exploit this.

## REAL SPHERICAL HARMONICS

Because we are concerned only with real surface quantities, we find it is more convenient to work with real spherical harmonics, $y_{lm}(\theta,\phi)$, expressed as linear combinations of the complex harmonics:

$$y_{lm}(\theta,\phi) = \begin{cases} (Y_{lm}(\theta,\phi) + Y_{lm}(\theta,\phi)^*)/\sqrt{2} \\ \quad \text{if } m > 0, \\ Y_{l0}(\theta,\phi) \\ \quad \text{if } m = 0, \\ -i\left(Y_{l\overline{m}}(\theta,\phi) - Y_{l\overline{m}}(\theta,\phi)^*\right)/\sqrt{2} \\ \quad \text{if } m < 0, \end{cases} \tag{14}$$

giving

$$y_{lm}(\theta,\phi) = \begin{cases} \vartheta_{lm}(\theta)(\cos m\phi)/\sqrt{\pi} \\ \quad \text{if } m > 0, \\ \theta_{lm}(\theta)/\sqrt{2\pi} \\ \quad \text{if } m = 0, \\ \vartheta_{l\overline{m}}(\theta)(\sin\overline{m}\phi)/\sqrt{\pi} \\ \quad \text{if } m < 0 \ (i.e., \ \overline{m} > 0). \end{cases} \tag{15}$$

Rotational symmetry is preserved in such linear combinations and the resulting real spherical harmonics also transform among themselves under rotation:

$$\hat{R}(\alpha\beta\gamma)\,y_{lm}(\theta,\phi) = \sum_{m'} y_{lm'}(\theta,\phi)R^{(l)}_{m'm}(\alpha\beta\gamma). \tag{16}$$

Consequently, the real expansion coefficients transform as

$$a'_{lm} = \sum_{m'} a_{lm'}R^{(l)}_{mm'}(\alpha\beta\gamma). \tag{17}$$

Expressions for the rotation of real spherical harmonics were given previously (e.g., Su and Koppens[27]), but we give our results here for complete-

ness because the form depends on the choice of the linear combination in eq. (14) and because it is convenient to have the rotation matrix elements listed explicitly. If eq. (14) is written as a sum

$$y_{lm}(\theta, \phi) = \sum_{m'} A^{(l)}_{mm'} Y_{lm'}(\theta, \phi), \qquad (18)$$

then for each order ($l$), the real rotation matrix, $R$, is given by

$$R = ADA^{\dagger} \qquad (19)$$

Recognizing that all nondiagonal elements of $A$ are zero, it is relatively straightforward but tedious to simplify eq. (19) symbolically. The result is

$$R^{(l)}_{m'm} = \begin{cases} d^{(l)}_{m'm}(\beta)\cos(m\gamma + m'\alpha) + (-1)^{m'} d^{(l)}_{\overline{m}'m}(\beta)\cos(m\gamma - m'\alpha); & m' > 0, m > 0; \\ d^{(l)}_{0m}(\beta)\sqrt{2}\cos(m\gamma); & m' = 0, m > 0; \\ (-1)^{m'+1} d^{(l)}_{m'm}(\beta)\sin(m\gamma + m'\alpha) + d^{(l)}_{\overline{m}'m}(\beta)\sin(m\gamma - m'\alpha); & m' < 0, m > 0; \\ d^{(l)}_{m'0}(\beta)\sqrt{2}\cos(m'\alpha); & m' > 0, m = 0; \\ d^{(l)}_{00}(\beta); & m' = 0, m = 0; \\ (-1)^{m'+1} d^{(l)}_{m'0}(\beta)\sqrt{2}\sin(m'\alpha); & m' < 0, m = 0; \\ (-1)^{m} d^{(l)}_{m'm}(\beta)\sin(m\gamma + m'\alpha) + (-1)^{m+m'} d^{(l)}_{\overline{m}'m}(\beta)\sin(m\gamma - m'\alpha); & m' > 0, m < 0; \\ (-1)^{m} d^{(l)}_{0m}(\beta)\sqrt{2}\sin(m\gamma); & m' = 0, m < 0; \\ (-1)^{m+m'} d^{(l)}_{m'm}(\beta)\cos(m\gamma + m'\alpha) + (-1)^{m+1} d^{(l)}_{\overline{m}'m}(\beta)\cos(m\gamma - m'\alpha); & m' < 0, m < 0. \end{cases} \qquad (20)$$

These expressions are consistent with the Su and Koppens formulas[27] and (by reusing partial results) are no more expensive to evaluate than the complex form [eq. (9)]. An option in our graphics program can display and rotate arbitrary real spherical harmonics [using eqs. (16) and (20)], and we visually verified that they rotate correctly. It should be noted that when $\beta = \gamma = 0$ we have a single rotation, $\alpha$, about the $z$ axis and the transformation of expansion coefficients is particularly simple. Because

$$d^{(l)}_{m'm}(0) = \delta_{m'm}, \qquad (21)$$

the coefficient transformation [eq. (17)] reduces to

$$a'_{lm} = a_{lm}\cos m\alpha + a_{l\overline{m}}\sin \overline{m}\alpha, \qquad (22)$$

as might be expected from symmetry. For a general rotation in which $\beta \neq 0$ the amount of computation can be reduced by using symmetries of the $d^{(l)}$ matrices[25]:

$$\begin{aligned} d^{(l)}_{m'm}(\beta) &= (-1)^{m'-m} d^{(l)}_{mm'}(\beta) \\ &= (-1)^{m'-m} d^{(l)}_{\overline{m}'\overline{m}}(\beta). \end{aligned} \qquad (23)$$

### Interpretation of Expansion Coefficients

The spherical harmonic expansion coefficients are sometimes referred to as ''shape descriptors'',[17,28] because the first few coefficients can be associated with specific geometric quantities. In an expansion of $r(\theta, \phi)$, the $l = 0$ coefficient encodes the average radius, or ''sea level''[14] of the surface, $\hat{r} = (4\pi)^{-1/2} a_{00}$, and the $l = 1$ coefficients describe the centroid of the surface, $\hat{\underline{x}} = (12\pi)^{-1/2}(a_{11}, a_{1\bar{1}}, a_{00})^T$. The coefficients up to $l = 2$ define an average ellipsoid. If the major axes of the ellipsoid are rotated into alignment with the coordinate axes, then the equation for an ellipsoid

$$\frac{x^2}{a^2} + \frac{y^2}{b^2} + \frac{z^2}{c^2} = 1, \qquad (24)$$

can be expressed in terms of a rotated radial expansion up to $L = 2$:

$$\left( \sum_{l=0}^{2} \sum_{m=-l}^{l} a'_{lm}\, y_{lm}(\theta, \phi) \right)^2 \times \left( \frac{\sin^2\theta\cos^2\phi}{a^2} + \frac{\sin^2\theta\sin^2\phi}{b^2} + \frac{\cos^2\theta}{c^2} \right) = 1. \qquad (25)$$

At $(\theta = \pi/2, \phi = 0)$ the only nonvanishing harmonics are of the form $\sin^m\theta\cos m\phi$ and we find

$$a = \sum_{l=0}^{2} a'_{l1}\, y_{l1}(\pi/2, 0). \tag{26}$$

Similarly, the remaining ellipsoidal radii are found from

$$b = \sum_{l=0}^{2} a'_{l\bar{1}}\, y_{l\bar{1}}(\pi/2, \pi/2), \tag{27}$$

$$c = \sum_{l=0}^{2} a'_{l0}\, y_{l0}(0, 0). \tag{28}$$

The ellipsoidal and coordinate axes can be aligned by finding, for example, the Euler rotation $(0\beta\gamma)$ that maximizes $c$, followed by a rotation, $(\alpha 00)$, to maximize $a$. Both rotations are determined numerically using a quasi-Newton method described below. Assuming that the ellipsoidal radii are distinct, they could be used as a nonsubjective way to place a set of molecules in a canonical orientation in space. Any potential ambiguity could be removed by examining terms to $l = 3$. However, we do not attempt to assign any geometric significance to coefficients above $l = 2$, other than to recall the notion of magnitude. For example, due to the unitarity of the rotation matrices, the integral

$$\int_0^{2\pi}\int_0^{\pi} r'(\theta, \phi)^2 \sin\theta\, d\theta\, d\phi = \sum_{lm} a'^2_{lm} = \sum_{lm} a^2_{lm} \tag{29}$$

is a rotational invariant that can be interpreted as the spherical component of the molecular surface area. If desired, the total molecular surface area can be calculated numerically from surface normals,

$$A = \int_0^{2\pi}\int_0^{\pi} |\underline{x}^{(\theta)}(\theta, \phi) \times \underline{x}^{(\phi)}(\theta, \phi)|\, d\theta\, d\phi, \tag{30}$$

where the superscripts denote partial differentiation. The ratio between the two areas could be used as a measure of the roughness of the surface.[29]

### Expressions for Spherical Harmonics

There are several ways in which the Legendre polynomials can be expressed. A recurrence relation is often recommended for numerical stability for very high order harmonics.[30,31] For example, the conventional recursion formula, modified to include the Condon–Shortley phase factor,[32] starts with

$$P_l^l(\theta) = (-1)^l \frac{(2l)!}{l!}\left(\frac{\sin\theta}{2}\right)^l \tag{31}$$

and continues down to $m = 0$ with[24]

$$P_l^m(\theta) = \frac{-2(m+1)\cot(\theta) P_l^{m+1}(\theta) - P_l^{m+2}(\theta)}{(l-m)(l+m+1)} \qquad m < l, \tag{32}$$

where $P_l^m(\theta) = 0$ when $m > l$. However, we find that a power series expression is easier to manipulate and faster to evaluate. We begin with the formula[24]

$$P_l^m(\mu) = \frac{(-1)^m}{2^l l!}(1-\mu^2)^{m/2}\frac{d^{l+m}}{d\mu^{l+m}}(\mu^2-1)^l, \tag{33}$$

where $\mu = \cos\theta$. Writing $(\mu^2 - 1)^l$ as a binomial expansion and differentiating it $l + m$ times, we obtain

$$P_l^m(\mu) = \frac{(-1)^m}{2^l l!}(l-\mu^2)^{m/2} \times \sum_{k=(l+m+1)/2}^{l} (-1)^{k+l}\binom{l}{k} \times \frac{(2k)!}{(2k-l-m)!}\mu^{2k-l-m}, \tag{34}$$

where the lower summation bound is taken using integer truncation. Collecting constant terms gives

$$\vartheta_{lm}(\theta) = (\sin\theta)^m \sum_{k=(l+m+1)/2}^{l} \nu_{lmk}[\cos\theta]^{2k-l-m}, \tag{35}$$

in which the coefficients, $\nu_{lmk}$, include the normalization factor [eq. (4)] and need only be calculated once. In our tests this expression was evaluated around twice as quickly as the equivalent recursive formulas. The analysis of Wiggins and Saito[30] indicates that the greatest errors in $P_l^m(\theta)$ are to be found near $\theta = \pi/4$, so the values of $\vartheta_{lm}(\pi/4)$ using eq. (35) (which was not included in the Wiggins and Saito[30] analysis) were compared with those calculated from the recursive formulas [eqs.

(31) and (32)]. The results agreed to 7 decimal places or better for all $l, m$ up to $l = 30$ when working in 64-bit floating point arithmetic. Considering the various approximations we make (described below), we are confident that the accuracy of the power series expression [eq. (35)] is well within the bounds of what we require.

### Trigonometric Caching

Much of the computational expense of using spherical harmonics is in repeated evaluation of the same or similar sine and cosine terms. One approach is to store precomputed values of $Y_{lm}$ in a grid of equally spaced polar coordinates,[17] although this gives a greatly increased point density toward the poles. Instead we use a more flexible empirical approach in which sine and cosine functions are calculated recursively [e.g., $\cos n\phi = 2\cos\phi\cos(n-1)\phi - \cos(n-2)\phi$ and $\sin n\phi = 2\cos\phi\sin(n-1)\phi - \sin(n-2)\phi$] and the results of such function calls, and powers thereof, are cached locally. A real function call is repeated only when necessary. By using basic identities such as $\cos(\alpha \pm \beta) = \cos\alpha\cos\beta \mp \sin\alpha\sin\beta$, this technique can also be used with the rotation matrix elements. For the small memory overhead of a cache for each angle ($\alpha\beta\gamma\theta\phi$) we obtain at least a threefold speed-up.

An alternative to repeatedly calculating the $d^{(l)}(\beta)$ matrices using the rather cumbersome formula eq. (10) is to relate the values of $d^{(l)}(\beta)$ to those of $d^{(l)}(\pi/2)$.[27,33] Surprisingly, however, we found this elegant approach to be slower than direct evaluation of eq. (10), despite using the above caching scheme.

## SURFACE SAMPLING

Two data structures are used to implement a fast and fair sampling of amolecular surface: a spherical triangular mesh and a spherical grid.

The triangular mesh is similar to the tessellation of the triangular faces of a regular icosahedron.[18,21] However, we inscribe the icosahedron in a sphere and use geodesic curves to divide the surface of the corresponding spherical triangles; we also allow any integral division of a triangular edge (the ''order'' of the mesh) to give a wider range of possible sampling densities. Connecting the centers of adjacent triangular faces gives the dual mesh, consisting of 12 pentagons separated by hexagons that cover the remainder of the surface. As a special case, a hexagonally snubbed dodecahedron (32 faces and 60 vertices, a soccer ball) is constructed from the icosahedral vertices and face centers. This data structure internally stores the coordinates and local connectivity of the icosahedral and dual vertices (which we call poles and nodes, respectively) of the two meshes. Specifically, a look-up table can find the three poles that neighbor a given node and the six (or five) nodes that neighbor a given pole. These relationships can be combined to implement a utility function that supplies approximately concentric rings of vertices that radiate away from a given seed vertex. This function, together with the spherical grid, is used to focus the sampling of the molecular surface.

There are many ways in which a spherical grid can be constructed. Because the grid is used to locate the nearest icosahedral mesh pole for a given $(\theta, \phi)$ coordinate, we require the grid to contain at least as many cells as there are icosahedral mesh poles and each grid cell to have an approximately equal area. Thus, the grid is built by setting the desired grid cell area to $a = 4\pi/N_{\text{poles}}$ and by dividing a hemisphere into $n$ latitudinal bands. The number of cells, $n_k$, in the $k$th band is derived from

$$n_k = \frac{2\pi}{a}\int_{\theta_{k-1}}^{\theta_k} \sin\theta d\theta. \quad (36)$$

to obtain

$$n_k = \lfloor 2\pi(\cos\theta_{k-1} - \cos\theta_k)/a + 1 \rfloor. \quad (37)$$

The first band, $\theta_1$, is found by setting $\theta_0 = 0$ and $n_1 = 1$. The total number of bands is set to $n = \lfloor 1/\theta_1 + 1 \rfloor$. Near the pole the first $p = \lfloor 0.1n \rfloor$ bands are found using

$$\theta_k = \arcsin(\sin\theta_1 + (k-1)/(p-1)(1-\sin\theta_1)) \quad p > 1. \quad (38)$$

Subsequent bands are spaced equally in $\theta$ over the remainder of the hemisphere. Dividing each band into cells using eq. (37) gives at least the required number of cells in the hemisphere. The grid cells of the second hemisphere are found by symmetry. This gives reasonably ''square'' grid cells even near the poles, as shown in Figure 1. The grid cell corresponding to any given $(\theta, \phi)$ coordinate can be found very quickly from the stored $\theta_k$ and $n_k$ data. The grid could also be used as the framework for the numerical integration of eq. (7), although a simpler and faster method is to use the icosahedral mesh, as described below.

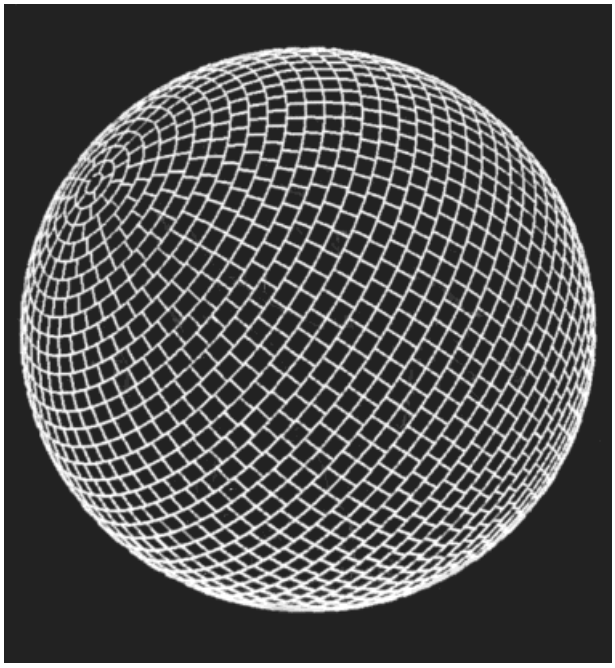

**FIGURE 1.** An example spherical grid of 2274 approximately equal area cells. This grid is used to map surface sample points onto icosahedral vertices during surface integration [eq. (40)].

When a single-valued surface is assumed, it is possible to use rays from the chosen origin to find estimates of the van der Waals surface, the solvent-accessible surface, and the molecular surface. A good estimate for the origin is the all-atom center of gravity. The $(\theta, \phi)$ coordinates of each atom, which are measured from this origin, give us a cell in the spherical grid that in turn points to a pole in the icosahedral mesh. The intersections between the atom and a ray from the origin to the pole are determined[18] and the largest solution along such a ray is saved as the radial distance from the origin at that angular sample point. This is repeated for concentric rings of icosahedral poles (above) until none of the rays of a ring cut the atom. Applying this procedure to each atom in turn and saving the maximum distance found for each sample ray gives a set of sample points of the van der Waals surface. If this procedure is applied when the radius of the probe sphere is added to each atom we obtain the solvent-accessible surface.[1] The molecular surface[2] is approximated by placing the probe sphere at each solvent-accessible surface sample point and applying the ray-atom intersection procedure to the probe sphere, this time saving the solutions that are nearest to the origin. This last step is essentially a modification of the technique originally described by Greer and Bush.[34]

Of these three surface types, the van der Waals surface is generally the least useful because it can contain deep but narrow cavities where occasionally a ray can reach far into the core of the molecule. In the context of a central projection, the molecular surface described above gives the most faithful representation of the surface shape and this surface is used in subsequent calculations. However, we stress that our procedure gives, by definition, only an approximation to the true molecular surface that would be obtained by rolling a probe sphere over the surface: when the algorithm is applied to multivalued surfaces it produces an enclosing envelope around each reentrant region.

## SURFACE INTEGRATION

Having obtained an unbiased distribution of molecular surface sample points at the icosahedral poles, a local smoothing operation is performed by setting the radial distance at each node of the dual mesh to be the average of the sample values found for its three neighboring poles. (The polar coordinates of the dual mesh remain unchanged.) The spherical harmonic coefficients are solved by representing the integral eq. (7), in terms of real harmonics, as a sum over the mesh nodes:

$$a_{lm} = \int_0^{2\pi} \int_0^{\pi} r(\theta, \phi)\, y_{lm}(\theta, \phi) \sin\theta d\theta d\phi \quad (39)$$

$$\simeq \sum_{n=1}^{N_{\text{nodes}}} r(\theta_n, \theta_n)\, y_{lm}(\theta_n, \theta_n) \Delta_n, \quad (40)$$

where $(\theta_n, \phi_n)$ are the polar coordinates of the $n$th mesh node and $\Delta_n$ is the triangular area associated with that node on the unit sphere, which was trivially obtained from the three neighboring poles. This novel way of approximating an integral over the sphere is justified by observing that in the limit of infinite tessellation each weight, $\Delta_n$, is (on average) effectively equivalent to the differential area element, $\sin\theta d\theta d\phi$. At moderate tessellation levels the area elements do not sum exactly to $4\pi$ so, although this error is small, eq. (40) is modified to include a normalizing correction:

$$a_{lm} \simeq \left( \frac{4\pi}{\sum_{n=1}^{N\text{nodes}} \Delta_n} \right) \sum_{n=1}^{N_{\text{nodes}}} r(\theta_n, \phi_n)\, y_{lm}(\theta_n, \phi_n) \Delta_n. \quad (41)$$

In practice, the coefficients, $a_{lm}$, are evaluated incrementally to exploit the behavior of the trigonometric cache with an outer loop over the mesh node coordinates and inner loops over $l$ and $m$. Compared to using an equiangular grid,[16,17] this approach can resolve the same level of detail with around a third fewer sample points.

## SURFACE MATCHING

If two molecular surfaces are positioned in a common coordinate system, one would expect to be able to find the rotation of one molecule relative to the other that minimizes some shape difference function, such as the root mean squared (RMS) distance difference between corresponding surface sample points. For example,

$$D_{\mathrm{RMS}} = \left[ \frac{1}{N_{\mathrm{nodes}}} \sum_{n=1}^{N_{\mathrm{nodes}}} (\underline{x}_1(\theta_n, \phi_n) - \underline{x}'_2(\theta_n, \phi_n))^2 \right]^{1/2}, \quad (42)$$

where the prime denotes rotation of the second molecule. Other similarity functions could be devised, but eq. (42) is particularly convenient because the orthonormality of the harmonic basis functions can be exploited by evaluating the corresponding integral

$$D^2 = \int_0^{2\pi} \int_0^{\pi} (\underline{x}_1(\theta, \phi) - \mathrm{x}'_2(\theta, \phi))^2 \sin\theta d\theta d\phi, \quad (43)$$

where $D^2 = 4\pi D^2_{RMS}$. Substituting for $\underline{x}$ and simplifying gives

$$D^2 = \int_0^{2\pi} \int_0^{\pi} \Big[ r_1(\theta, \phi)^2 + r'_2(\theta, \phi)^2 - 2 r_1(\theta, \phi) r'_2(\theta, \phi) \Big] \sin\theta d\theta d\phi, \quad (44)$$

which can be trivially integrated [eq. (29)],

$$D^2 = \sum_{lm} a^2_{lm} + \sum_{lm} b'^2_{lm} - 2 \sum_{lm} a_{lm} b'_{lm}; \quad (45)$$

and because the second sum is rotationally invariant [eq. (29)],

$$D^2 = \sum_{lm} (a^2_{lm} + b^2_{lm} - 2 a_{lm} b'_{lm}). \quad (46)$$

This expression is essentially the same as the shape similarity measure given by Leicester et al.[17] However, our development gives the expression a physical basis and it shows how the effect of translation can be accommodated. Translation of one molecule relative to the other may be necessary to obtain the absolute minimum in the surface distance difference, because (without prior knowledge) the choice of molecular origin is unlikely to coincide with the centroid of the harmonic surface. If eq. (43) is modified to include translations of the surface centroids (applied after any rotation about the origin), we then have

$$D^2 = \int_0^{2\pi} \int_0^{\pi} ((\underline{x}_1(\theta, \phi) - \hat{\underline{x}}_1) - (\underline{x}'_2(\theta, \phi) - \hat{\underline{x}}_2))^2 \sin\theta d\theta d\phi. \quad (47)$$

After some similar working and using $\hat{\underline{x}}_1 = (12\pi)^{-1/2}(a_{11}, a_{1\bar{1}}, a_{00})^T$, etc., we obtain a general analytic shape similarity expression:

$$D^2 = \sum_{l=0}^{L} \sum_{m=-l}^{l} (a^2_{lm} + b^2_{lm} - 2 a_{lm} b'_{lm}) + 1/3 \sum_{m=-1}^{+1} \Big[ (a_{1m} - b_{1m})^2 - 2(a_{1m} - b'_{1m})(a_{1m} - b_{1m}) \Big]. \quad (48)$$

Determining the rotation that gives the global minimum of eq. (48) is described in the next section.

## DISTANCE MINIMIZATION

Relative to the $l = 0$ sea level, a spherical harmonic molecular surface to order $L$ has $(L + 1)^2 - 1 = L(L + 2)$ independent coefficients; so a given surface expansion can be expected to contain at most this number of surface features (''knobs and holes''). If minimization of the distance function is applied when $L$ is large, there is a high probability of becoming trapped in a local minimum. Because we know that the low resolution terms contribute to the bulk of the shape, it is reasonable to begin the search at low resolution, typically with $L = 5$. On the other hand, if only low resolution surfaces are compared, it is possible that the true global minimum may be missed. Thus, a two-step minimization procedure is used as follows.

In the first step the rotation space is sampled using the spherical coordinates of a low resolution icosahedral tessellation of either 32 or 60 vertices (from our soccer ball). This assigns rotation angles to $\beta$ and $\gamma$. The expansion coefficients are rotated through $(0\beta\gamma)$ [using eq. (17)] and then by eight equal steps in $\alpha$ [in order to use eq. (22)], evaluat-

ing the distance function, $D^2$, at each orientation. Conceptually, each icosahedral vertex is rotated onto the north pole, followed by further rotations about the north–south axis; this gives a fairer coverage of the parameter space than using equal angular increments. In the second step the quasi-Newton function minimization method of Broyden, Fletcher, Goldfarb, and Shanno[35] is used to simultaneously solve for the Euler rotation angles that take a given starting guess to a nearby local minimum in the distance function. This is applied only to the 20 most promising trial orientations from the initial sampling step. However, several starting guesses may converge to essentially the same solution, although this may not be apparent from direct inspection of the Euler angles. Such degenerate solutions are detected and eliminated by converting the Euler rotation angles into an equivalent single rotation, $\chi$, about a unit axis, $\underline{u}$,

$$\hat{R}(\chi, \underline{u}) = \underline{R}(\alpha, \beta, \gamma), \tag{49}$$

where $\chi$ and $\underline{u}$ can be found directly from the matrix elements of the Cartesian rotation matrix, $\underline{R}(\alpha, \beta, \gamma)$.[25] Two rotations are considered degenerate if they resolve to the same axial rotation to within a given tolerance. Testing for $\arccos(\underline{u}_1 \cdot \underline{u}_2) \leq 10^\circ$ and $|\chi_2 - \chi_1| \leq 10^\circ$ generally works well. To distinguish between distinct orientations that have similar distance scores, the minimization procedure is repeated on the remaining solutions at higher harmonic resolutions. The best orientation ought to score well at all orders of expansion, whereas ''false positives'' may appear at low resolution but score poorly with higher order terms. As an optimization we use a simple bracketing procedure to eliminate the worst of the local minima after each round of minimization. The same general procedure is used to determine the molecular ellipsoid described above, although here the search space is much flatter and fewer starting guesses are required.

## Results

We tested our surface matching procedure using a number of antibody variable domains whose coordinates are available in the PDB.[36] As an example, we give results obtained using the VH domains of HyHel-5[37] and KOL[38] (PDB codes 3HFL and 2IG2, respectively). Similar results were also obtained with light chain variable domains.

**TABLE I.**
**Spherical Harmonic Molecular Surface Generation, Coefficient Rotation, and Surface Display Times for HyHel-5 VH Domain.**

| Order | Integration | Rotation | Display |
|---|---|---|---|
| 5 | 1.2 (2.5) | 0.001 (0.01) | 0.6 (1.4) |
| 10 | 3.5 (12.0) | 0.04 (0.12) | 2.0 (6.9) |
| 20 | 15.3 (71.8) | 0.18 (0.58) | 8.3 (35.9) |
| 30 | 39.0 (215) | 0.70 (2.31) | 21.0 (107) |

The values were calculated using 2252 molecular surface sample points (taking 3.15 s) of an order 14 icosahedral mesh (4500 nodes). Times are elapsed seconds measured on a Silicon Graphics Indy workstation with an R4600 floating point coprocessor. The values in parentheses are for the corresponding calculation without trigonometric caching.

Generating an order 14 icosahedral mesh (2252 poles, 4500 nodes) and the corresponding spherical grid takes around 0.75 s on a Silicon Graphics Indy workstation with an R4600 floating point coprocessor. (All timings are of elapsed time on this platform.) When using these data structures it takes 3.15 s to sample the surface of the first 105 residues (844 non-hydrogen atoms) of the VH domain of HyHel-5 to give a relatively low sample density molecular surface with an average angular sample spacing of around 4.6° and an average triangle area of 1.13Å$^2$. Calculating the harmonic expansion coefficients over the 4500 nodes takes 3.5 s for an $L = 10$ expansion, although higher order surfaces take significantly longer as can be seen from Table I. We find $L = 9$ is usually sufficient for surface matching, and such a low resolution surface can be calculated and displayed in under 10 s using our program. The highest resolution surface that we calculated uses an order 30 mesh (9612 poles, 19,220 nodes), which takes 20 s to sample, and an $L = 30$ harmonic expansion takes a further 164 s to calculate. This last example is approaching the resolution that would be obtained with a 1° equiangular grid.[16,17] Table I shows a similar performance trend with the general Euler angle rotation of harmonic expansion coefficients and with the generation (display) of the surface from the shape coefficients. However, the time taken to rotate the expansion coefficients about only the $z$ axis [eq. (22)] is almost negligible.

When comparing two molecular surfaces (in this case the VH domains of HyHel-5 and KOL) using the procedure described above, the first rotational sampling step at $L = 5$ takes 0.46 s to generate distance values for all of the $60 \times 8 = 480$ sample orientations. The 20 best candidate orienta-

tions are minimized and filtered in three stages (at $L = 5, 7$, and 9), taking a further 2 s to evaluate another 394 distance functions to give three possible solutions. The best solution is shown in Figures 2–4. A similar but inferior match can be found without using function minimization, but this requires $500 \times 20 = 10{,}000$ trial orientations and the elapsed time increases to 16 s.

With antibody domains the all-atom center of mass is a good estimate of the spherical harmonic surface centroid, the two points being separated by around 1 or 2Å. Thus, the choice of distance function [eq. (46) or (48)] makes little difference to the relative molecular orientations in the best surface superposition. However, when translation is included, using eq. (48), the absolute distance difference can be reduced by up to 25%. We expect this would be an important effect if multiple surfaces are to be compared.

With very similar molecular shapes where we know the expected solution, we often find that the ''right'' solution is immediately found as the one with the smallest distance difference after minimization at $L = 5$. Subsequent minimization at higher order terms reduces the distance difference but has very little impact on the rotation angles as

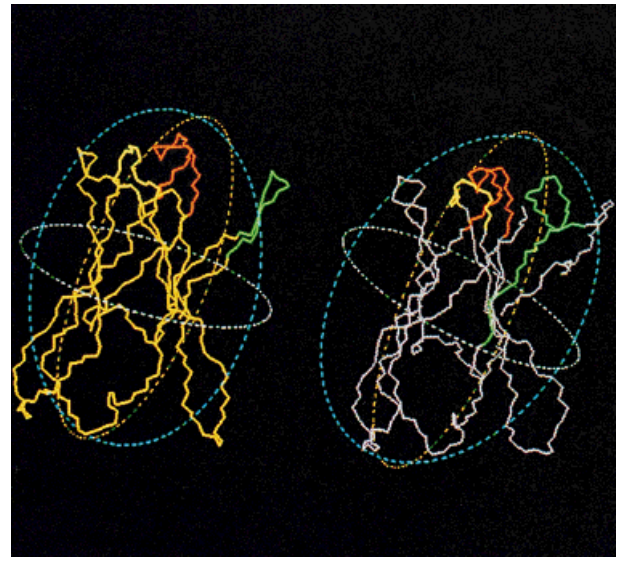

**FIGURE 3.** The backbone traces of the HyHel-5 (left) and KOL (right) VH domains after minimizing spherical harmonic surfaces at order $L = 9$ (separated for clarity). The hypervariable CDR loops are highlighted toward the top of each molecule. The average molecular surface ellipsoid is also shown for each domain. Considering the relative orientations of the ellipsoidal axes, it is clear that aligning only the ellipsoids (i.e., terms to $L = 2$) would not give the correct superposition.

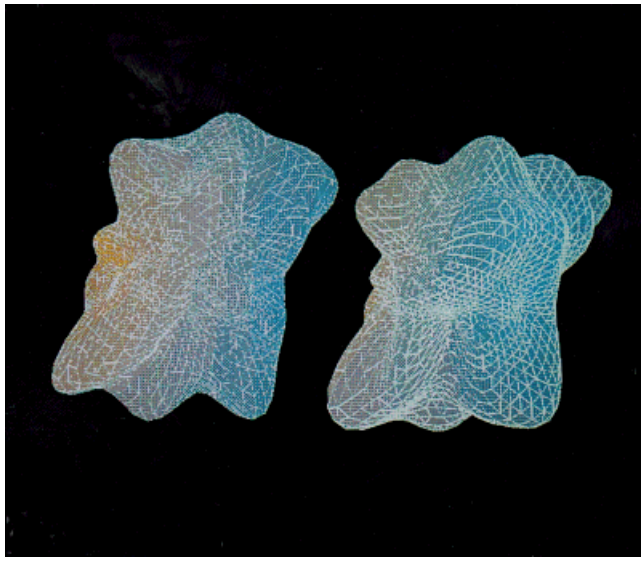

**FIGURE 2.** Maximally aligned spherical harmonic molecular surfaces of the HyHel-5 (left) and KOL (right) antibody VH domains, which are separated by 35Å for clarity. These surfaces are displayed at order $L = 12$, although the superposition was calculated only up to $L = 9$.

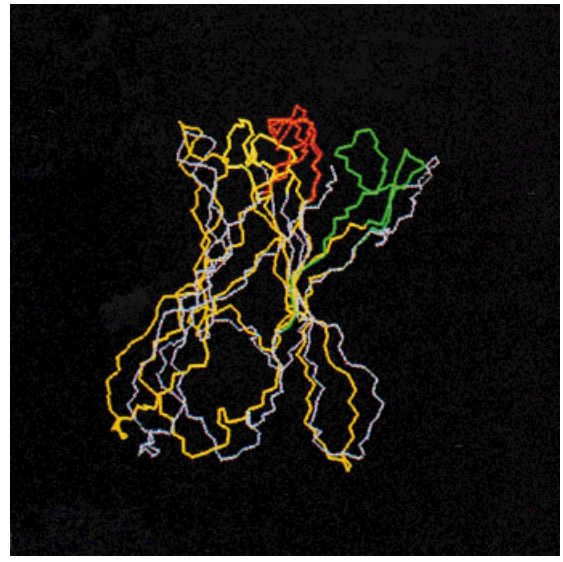

**FIGURE 4.** The backbone traces of the HyHel-5 and KOL VH domains superposed after minimizing spherical harmonic surfaces at order $L = 9$.

the solutions tend to dither around the low order orientation. With less similar shapes we find that the best solution may be missed if the search begins with fewer than 60 ⊗ 8 sample icosahedral orientations. This was found to be a sufficient number of starting guesses to be confident that the solution lies within the top 20 trial orientations, but now minimization at higher order terms is required to ensure that the solutions are ranked correctly.

## Discussion

The procedures described above allow efficient computation, rotation, and comparison of arbitrary spherical harmonic surface properties. A spherical harmonic parametrization is useful because it removes, in a controllable way, much of the complicated detail of the original shape and because the resulting analytic surface is well behaved when using established numerical methods such as function minimization. This behavior can be exploited by minimizing a distance function between a pair of macromolecular shapes to find the relative orientation that gives the best superposition of the two surfaces. We showed that this can be done using fairly low resolution harmonic terms generated from a moderately sparse set of surface sample points; thus, we were able to match a pair of macromolecular surfaces in just a few seconds on a modern workstation.

This interactive level of performance is possible because of a number of features in our approach. The use of a power series expression for the real spherical harmonic basis functions and a simple trigonometric caching scheme allow the overall amount of computation to be significantly reduced. The main benefit, however, comes from the use of a tessellated icosahedron that allows a fast and fair sampling of the molecular surface and provides a simple numerical integration method of determining the harmonic expansion coefficients. Table I shows that our integration algorithm takes only around twice the time needed to reconstruct an encoded surface for display. By comparison, subsequent rotation of low order coefficients is relatively inexpensive, thus allowing a rapid evaluation of the distance function at different orientations. The icosahedral tessellation is also useful here because it allows a fair sampling of the rotational search space so that the distance minimization algorithm need only be applied to a small number of promising trial orientations.

For simplicity we chose to generate surfaces directly from the 3-D structures. The procedure that does this is fast and robust, and the assumption of a single-valued surface for antibody domains does not compromise the shape matching algorithm. Thus, we expect that these methods could be used successfully with many other types of globular protein domains. They could also be used to compare (and perhaps classify) complete antibody Fv fragments or (by integrating over surface patches) perform a more detailed comparison of just the antigen combining sites.[39] Additionally, because our approach extends the principles of Chau and Dean's gnomonic projection method,[18] we expect that our techniques would also be applicable to the comparison of smaller molecules such as neurotoxins[18] and antibiotics.[40]

In principle, matching molecular shapes using spherical harmonic surfaces is similar to other small-molecule multipole matching techniques.[41, 42] These methods tend to use low order multipoles (i.e., $L = 2$ or 3) whereas our results indicate that harmonic expansions of between $L = 5$ and $L = 9$ are needed for a good surface match; hence, an efficient rotational sampling strategy is required to distinguish between the many local minima. However, to obtain an accurate spherical harmonic parametrization of reentrant surfaces and nonglobular molecules it would first be necessary to stretch a molecular surface onto the sphere, which can be an expensive operation.[16, 28]

Our approach to shape comparison is also similar to the fast Fourier transform (FFT) docking correlation technique of Katchalski−Katzir et al.,[43] which can be considered in terms of simulating translations of one molecule about a second, stationary molecule using the rotational properties of the complex exponential basis functions. It is interesting to note that in current FFT docking algorithms a new FFT must be calculated for each rotational increment of the stationary molecule, and this contributes significantly to the computational cost of applying FFT techniques to the protein docking problem.[43, 44] Work is in progress to eliminate this overhead by expressing the docking correlation in terms of spherical harmonic and radial basis functions to give a full 6-D docking correlation that requires only two shape parametrizations to initialize the calculation (in preparation).

## Conclusions

We demonstrated how some of the computational expense of using a spherical harmonic surface parametrization can be alleviated. Once the coefficients of a spherical harmonic molecular surface have been determined, they offer a representation that is relatively easy to operate on, particularly when the task is one of search in a rotational search space. By mapping the surface shape matching problem into a spherical harmonic basis we obtain an analytic RMS shape difference expression that can be minimized by rotating only the harmonic expansion coefficients. Our calculations show that a pair of similar molecular surfaces can be rapidly and accurately rotated into superposition by considering only the gross surface features encoded by a moderate number of spherical harmonic terms. This demonstrates the utility of using spherical harmonic surfaces, and we suggest that such low resolution parametrizations may be of practical use in the design of small ligands and in the study of macromolecular interactions.

## Software Availability

The program described is available on the internet at http://www.biochem.abdn.ac.uk/hex/.

## Acknowledgments

We thank Prof. J. E. Fothergill for several useful discussions during the preparation of this manuscript. D.W.R. is grateful for a Special Studentship from the Chemicals Pharmaceuticals Directorate of the BBSRC.

## References

1. Lee, B.; Richards, F. M. J Mol Biol 1971, 55, 379–400.
2. Richards, F. M. Annu Rev Biophys Bioeng 1977, 6, 151–176.
3. Connolly, M. L. Science 1983, 221, 709–713.
4. Connolly, M. L. J Appl Crystallogr 1983, 16, 548–558.
5. Connolly, M. L. J Appl Crystallogr 1985, 18, 499–505.
6. Lee, R. H.; Rose, G. D. Biopolymers 1985, 24, 1613–1627.
7. Connolly, M. L. J Mol Graphics 1986, 4, 3–6.
8. Connolly, M. L. Biopolymers 1986, 25, 1229–1247.
9. Jiang, F.; Kim, S. J Mol Biol 1991, 219, 79–102.
10. Lin, S. L.; Nussinov, R. J Mol Graphics 1996, 14, 78–90.
11. Helmer–Citterich, M.; Tramontano, A. J Mol Biol 1994, 235, 1021–1031.
12. Lin, S. L.; Nussinov, R.; Fischer, D.; Wolfson, H. J. Proteins 1994, 18, 94–101.
13. Norel, R.; Lin, S. L.; Wolfson, H. J.; Nussinov, R. J Mol Biol 1995, 252, 263–273.
14. Wodak, S. J.; Janin, J. J Mol Biol 1978, 124, 323–342.
15. Max, N. L.; Getzoff, E. D. IEEE Comput Graphics Appl 1988, 8(4), 42–50.
16. Duncan, B. S.; Olson, A. J. Biopolymers 1993, 33, 219–229.
17. Leicester, S.; Finney, J.; Bywater, R. J Math Chem 1994, 16, 315–341.
18. Chau, P. L.; Dean, P. M. J Mol Graphics 1987, 5, 97–100.
19. Eisenhaber, F.; Lijnzaad, P.; Argos, P.; Sander, C.; Scharf, M. J Comput Chem 1995, 16, 273–284.
20. Bladon, P. J Mol Graphics 1989, 7, 130–137.
21. Duncan, B. S.; Olson, A. J. J Mol Graphics 1995, 13, 250–257.
22. Duncan, B. S.; Olson, A. J. J Mol Graphics 1995, 13, 258–264.
23. Leicester, S.; Finney, J.; Bywater, R. J Math Chem 1994, 16, 343–365.
24. Hobson, E. W. The Theory of Spherical and Ellipsoidal Harmonics; Cambridge University Press: London, 1931.
25. Biedenharn, L. C.; Louck, J. C. Angular Momentum in Quantum Physics; Addison–Wesley: Reading, MA, 1981.
26. Leicester, S. E.; Finney, J. L.; Bywater, R. P. J Mol Graphics 1988, 6, 104–108.
27. Su, Z. W.; Coppens, P. Acta Crystallogr 1994, A50, 636–643.
28. Brechbuhler, C.; Gerig, G.; Kubler, O. Comput Vision Image Understanding 1995, 61, 154–170.
29. Zachmann, C. D.; Kast, S. M.; Sariban, A.; Brickmann, J. J Comput Chem 1993, 14, 1290–1300.
30. Wiggins, R. A.; Saito, M. Bull Seismol Soc Am 1971, 61, 375–381.
31. Libbrecht, K. G. Solar Phys 1985, 99, 371–373.
32. Condon, E. U.; Odabasi, H. Atomic Spectra; Cambridge University Press: Cambridge, U.K., 1980.
33. Edmonds, A. R. Angular Momentum in Quantum Physics; Princeton University Press: Princeton, NJ, 1974.
34. Greer, J.; Bush, B. L. Proc Natl Acad Sci 1978, 75, 303–307.
35. Fletcher, R. Practical Methods of Optimisation, Vol. 1; Wiley: New York, 1980.
36. Bernstein, F. C.; Koetzle, T. F.; Williams, G. J. B.; Mayer, E. F., Jr.; Bryce, M. D.; Rodgers, J. R.; Kennard, O.; Shimanouchi, T.; Tasumi, M. J Mol Biol 1977, 112, 535–542.
37. Cohen, G. H.; Sheriff, S.; Davies, D. R. Acta Crystallogr 1996, D52, 315–326.
38. Kratzin, H. D.; Palm, W.; Stangel, M.; Schmidt, W. E.; Friedrich, J.; Hilschmann, N. Biol Chem 1989, 370, 263–272.
39. Gerstein, M. Acta Crystallogr 1992, A48, 271–276.
40. Blaney, F.; Finn, P.; Phippen, R. W.; Wyatt, M. J Mol Graphics 1993, 11, 98–105.
41. Grant, J. A.; Gallardo, M. A.; Pickup, B. T. J Comput Chem 1996, 17, 1653–1666.
42. Silverman, B. D.; Platt, D. E. J Med Chem 1996, 39, 2129–2140.
43. Katchalski–Katzir, E.; Shariv, I.; Eisenstein, M.; Friesem, A. A.; Aflalo, C. Proc Natl Acad Sci 1992, 89, 2195–2199.
44. Gabb, H. A.; Jackson, R. M.; Sternberg, M. J. E. J Mol Biol 1997, 272, 106–120.